Journal of Nuclear Materials 393 (2009) 409–417

Contents lists available at ScienceDirect

Journal of Nuclear Materials

journal homepage: www.elsevier.com/locate/jnucmat

Modeling dislocation structure development and creep–swelling coupling in neutron irradiated stainless steel

A.A. Semenov [a,b], C.H. Woo [a,*]

[a] Department of Electronic and Information Engineering, The Hong Kong Polytechnic University, Kowloon, Hong Kong SAR, China
[b] On Leave from Institute for Nuclear Research, Russian Academy of Sciences, Moscow, Russia

ARTICLE INFO

Article history:
Received 29 March 2009
Accepted 22 June 2009

PACS:
61.80.Az
61.82.Bg
62.20.Hg

ABSTRACT

Anisotropic nucleation and growth of multi-classes of dislocation loops under the combined actions of fast-neutrons and an external applied stress are considered in modeling dislocation structure development in metals and alloys. The stochastic nature of the nucleation kinetics is formulated via the Fokker–Planck equation. The strain derived from the climb of the anisotropic dislocation structure is separable into volumetric and deviatoric components, corresponding respectively to swelling and creep. The creep contribution resulting from the development of the stress-induced dislocation anisotropy is found to be very significant and exhibits a strong correlation with swelling. For stainless steel, our model explains very well the complex deformation behavior observed in a wide variety of in-reactor experiments.

1. Introduction

Microstructure record left by an applied stress in stainless steels during irradiation is often found characterized by an anisotropic dislocation structure [1–5]. This is evident [5] of the operation of stress-induced preferred absorption (SIPA) [6–11], a mechanism that may produce irradiation deformation both directly and indirectly. Directly, deviatoric strain is produced by the differential climb speeds of dislocations with different orientations due to the stress-induced bias differential. The associated creep rate is directly calculable based on point-defect properties obtainable from atomistic methods [6], and has been the focus of most irradiation creep studies [7–11]. Indirectly, the stress-induced differential climb creates an anisotropic dislocation structure [4,5], which causes deformation via a mechanism called SIPA-induced growth (SIG) [12]. Theoretical estimates indicate that the associated strain rate is sensitive to the swelling rate, with magnitudes that may be very significant [12–14].

Experimentally, in-reactor deformation measurements in stainless steels [15–25] indeed exhibit two components, one independent of swelling and the other coupled to swelling and has a strain rate directly proportional to the swelling rate. In addition, irradiation creep is often observed to be accompanied by an anisotropic dislocation structure [5,20–25]. At the same time, the strain rate usually persists for a substantial period of time, even after the applied stress is removed [5]. These observations are strongly reminiscent of the operation of SIG.

Most theories on irradiation-induced deformation have focused on the direct component [7–11]. The indirect component is difficult to calculate, absent a good theory for interstitial loop nucleation under an applied stress. Any investigation in this respect has to be limited to qualitative studies based on simplifying assumptions [12–14].

Recent developments in the theory of nucleation kinetics [26,27] provide a good basis for treating the high sensitivity of nucleation events to the net point-defect flux. The successful modeling of nucleation and growth of dislocation loops in unstressed samples in [26,27] helps explain dislocation structure development with production bias [28] operating. In the present paper, this theory is extended to treat the nucleation and growth of multi-classes of differently oriented dislocation loops in the development of dislocation structure under an applied stress.

The objective of this paper is to holistically study irradiation deformation in stainless steels, particularly the coupling between creep and swelling associated with dislocation structure development under an applied stress. Comparing the calculated results with the experimental ones in the literature, we also hope to clarify the role of the stress-induced anisotropy of the dislocation structure in the complex deformation behavior of stainless steels under stress in a fast-neutron flux. Finally, the comparison may also test the predictive capability of our dislocation structure development model in the presence of an applied stress.

* Corresponding author. Tel.: +852 2766 6646.
E-mail address: chung.woo@polyu.edu.hk (C.H. Woo).

0022-3115/$ - see front matter © 2009 Elsevier B.V. All rights reserved.
doi:10.1016/j.jnucmat.2009.06.021

2. Formulation

2.1. Preliminary considerations

Under cascade damage conditions of a fast-neutron flux, we have to face the complication that a significant fraction of primary interstitials produced are retained in clusters. Recognition of this fact has led to the introduction of the production bias concept [28]. This concept is based on the premise that point defects in clusters do not participate in the conventional segregation of interstitials and vacancies via preferential attraction of single interstitials to dislocations. However, within this concept, the commonly observed network formation via the nucleation and growth of sessile Frank interstitial loops does not seem plausible. Indeed, at elevated temperatures, vacancy clusters are thermally unstable, so that the supersaturation of single vacancies is higher than that of the single interstitials. The mean net vacancy flux received by the thermally stable primary interstitial clusters makes nucleation impossible without statistical variations. In reality, however, the net vacancy flux fluctuates because of the stochastic nature of migratory jumps and cascade initiation, so that interstitial loop nucleation and growth is not a deterministic, but a probabilistic event. In this connection, a stochastic treatment such as followed in [26,27] is necessary. To consider the action of external stress, this approach can be extended to take into account the loop orientation dependence of the nucleation rate. The details will be discussed in the following subsection.

In a related issue, the effects of one-dimensional transport of small interstitial clusters [29–31] observable in computer simulations in pure metals [32] on interstitial loop nucleation and growth should be considered. However, the invariable presence of compositional disorder in the crystal lattice due to alloying and various thermal–mechanical treatment may lead to the trapping or scattering of the clusters [6,33–35], drastically reducing the likelihood of long-range one-dimensional transport of interstitial defects. Moreover, recent investigations [36,37] showed that void lattice formation in "pure" metals cannot occur if more than ~1% of the interstitial atoms undergo one-dimensional diffusion. The development of large-scale heterogeneous void swelling found near grain boundaries and dislocation walls can also be understood without invoking the one-dimensional diffusion [38–40]. Most importantly, the majority of void swelling models that have stood the test of decades of experiments do not require the involvement of 1-D SIA kinetics. All these suggest that the inclusion of one-dimensional diffusion in irradiation-damage studies may not always be necessary. Accordingly, we neglect the effects of the 1-D diffusion SIA component in the present paper.

Small interstitial clusters coalesce with faulted loops during climb, and may also serve as a source of interstitials to their growth. This is clear from the in situ observations in dual-beam experiments of Jenkins [41]. Indeed, both numerical [42] and analytical [26,27] calculations show that sufficiently large interstitial loops may grow under the combined action of the dislocation bias and continuous loop coalescence, despite the net vacancy flux that they receive. The swelling produced by loop growth in this way is in quantitative agreement with experiments [26,42].

2.2. Evolution equations of the Frank loops

Different populations of Frank interstitial loops and network dislocations of different classes have different dislocation biases according to their orientations with respect to the applied stress [11]. The governing equation for evolution of the Frank loop population of each class is similar to that previously derived for the case of a single class of dislocations [26,42–43]. With the last two terms describing the creation and annihilation of loops in the population, the evolution of the kth loop class can be described by the Fokker–Planck equation:

$$\frac{\partial f_{ik}(n,t)}{\partial t} = -\frac{\partial}{\partial n}\left\{V_{ik}(n) - \frac{\partial}{\partial n}D_{ik}(n)\right\}f_{ik}(n,t) + \frac{\varepsilon_{ik}G}{n_{ig}}\delta(n-n_{ig}) - \left.\frac{\partial f_{ik}(n,t)}{\partial t}\right|_{\text{loss}} \quad (1)$$

Here $f_{ik}(n, t)$ is the distribution function of interstitial loops of the kth class in the space of loop sizes n at time t. Small immobile interstitial clusters continuously generated in collision cascades are considered as interstitial loop embryos. In the spirit of the production bias theory [28], the formation of loop embryos are assumed to be intra-cascade events, and the initial sizes, n_{ig}, of the loop embryos are the same for all loop classes, as reflected by the δ-function in Eq. (1). They are treated as small dislocation loops of radius $r_i = (n\Omega/\pi b)^{1/2}$, where n is the number of interstitials in the cluster, Ω is the atomic volume, b is the Burgers vector. The rate of generation of embryos in collision cascades is given by $\varepsilon_{ik}G/n_g$, where G is the *effective* generation rate of point defects both in cluster and free form [28], and ε_{ik} is the fraction of interstitials forming embryonic loops of the kth class.

The "diffusivity" $D_{ik}(n)$ in Eq. (1) describes the stochastic spread of the size distribution of interstitial loops in time due to random fluctuations in the point-defect fluxes [43,44],

$$D_{ik}(n) = D^s_{ik}(n) + D^c_{ik}(n), \quad (2)$$

with

$$D^s_{ik}(n) = \left(\frac{\pi n}{\Omega b}\right)^{1/2}(Z_{ik}D_iC_i + Z_{\nu k}D_\nu C_\nu), \quad (3)$$

$$D^c_{ik}(n) = \frac{N_d G n}{4b}\left[Z^2_{\nu k}\frac{\langle N^2_{d\nu}\rangle}{k_\nu N^2_d} + Z^2_{ik}\frac{\langle N^2_{di}\rangle}{k_i N^2_d}\right], \quad (4)$$

where Z_{jk} ($j = i, \nu$) is the reaction constant between the loop of the kth class and point defects, C_j and D_j are respectively the average concentration of point defects and their diffusion coefficient. N_d is the average number of point defects generated per cascade both in cluster and free form, $\langle N^2_{dj}\rangle$ is the average square of the number of vacancies and interstitials generated per cascade. We also denote the total sink strength for vacancies by $k_\nu{}^2$, and for mobile interstitials by $k_i{}^2$. The two terms on the right-hand side of (2) are, respectively, the contribution to D_{ik} due to the randomness of the point-defect jumps, and that of the cascade initiation [43,44].

The "drift velocity" $V_{ik}(n)$ consists of the two terms. The first one is given by the conventional expression for the growth rate of interstitial loops due to point-defect absorption:

$$V_{ik}(n)|_{pd} = \frac{2\pi r_i(n)}{\Omega}(Z_{ik}D_iC_i - Z_{\nu k}D_\nu C_\nu). \quad (5)$$

The second one represents the rate of change in the loop size due to the absorption of smaller loops by coalescence and has the following form [26,42]:

$$V_{ik}(n)|_{cls} = \frac{2\pi r_i(n)}{\Omega}\int_{n_{\min}}^{n} x f_{ik}(x,t)W_k(x,n)dx \quad (6)$$

Here $n_{\min}$ is the size of interstitial clusters at which they become mobile. According to Eq. (6), in the present approach the loop coalescence is restricted only to the coalescence of the loops with the same orientation.

The coalescence between loops of sizes n' and n ($n' < n$) is described by the reaction constant $W_k(n',n)$ [26,42],

$$W_k(n',n) = \frac{4r_i(n')}{b}\left[D_{lk}(n) + (D^2_{lk}(n) + V^2_{lk}(n)b^2/4)^{1/2}\right], \quad (7)$$

In Eq. (7), the reaction distance between the coalescing loops is assumed to be equal to the radius of smaller loop $r_i(n')$, V_{lk} is the average climb velocity of the loop segments, i.e.,

$$V_{lk}(n) = \frac{1}{b}(Z_{ik}D_iC_i - Z_{vk}D_vC_v) + \frac{1}{b}\int_{n_{\min}}^{n} xf_{ik}(x,t)W_k(x,n)dx. \quad (8)$$

$D_{lk}(n)$ is the climb "diffusion coefficient" due to the fluctuating point-defect fluxes. Similar to Eq. (2), D_{lk} can be written as [26,42]:

$$D_{lk}(n) = D^s_{lk}(n) + D^c_{lk}(n), \quad (9)$$

$$\text{with} \quad D^s_{lk}(n) = \frac{\Omega}{4\pi b^2 r_i(n)}[Z_{vk}D_vC_v + Z_{ik}D_iC_i], \quad (10)$$

$$D^c_{lk} = \frac{N_d G\Omega}{16\pi b^2}\left[Z^2_{vk}\frac{\langle N^2_{dv}\rangle}{k_v N^2_d} + Z^2_{ik}\frac{\langle N^2_{di}\rangle}{k_i N^2_d}\right]. \quad (11)$$

Note that D^c_{lk}, unlike D^s_{lk}, is not directly related to the loop size.

Coalescence results in fewer loops. From Eq. (6), the law of matter conservation dictates that the last term in Eq. (1), which describes the loss of loops due to their coalescence, has to have the form [42]

$$\left.\frac{\partial f_{ik}(n,t)}{\partial t}\right|_{\text{loss}} = f_{ik}(n,t)\left\{\frac{2\pi}{\Omega}\int_n^{n_m} W_k(n,n')r_i(n')f_{ik}(n',t)dn' + W_k(n,n_m)\rho_{dk}\right\}, \quad (12)$$

where n_m denotes the size of the loops at which they unfault and join the network, ρ_{dk} is the line density of network dislocations of the kth class. The last term of Eq. (12) describes the absorption of loops by network dislocations.

To establish the boundary conditions for the evolution equations, we assume that small clusters consisting of less than three self-interstitials are 3-D mobile. Thus, interstitial clusters shrinking below the minimum size $n_{\min}$ are not loop embryos any longer. This condition is translated in the corresponding left boundary condition for the Fokker–Planck equation (1), i.e.,

$$f_{ik}(n_{\min}, t) = 0. \quad (13)$$

Assuming that a loop growing beyond the size $n_{\max}$ becomes incorporated into the network, we can also write the right boundary condition, similarly to Eq. (13),

$$f_{ik}(n \geqslant n_m, t) = 0. \quad (14)$$

According to the evolution Eq. (1) and the boundary conditions Eqs. (13), (14), the total number of interstitials $Q_{ik}(t)$ accumulated in loops of kth class is governed by the following simple law of matter conservation:

$$\frac{dQ_{ik}(t)}{dt} = \frac{d}{dt}\int_{n_{\min}}^{n_m} nf_{ik}(n,t)dn = G\varepsilon_{ik} + n_{\min}J^{ss}_{ik}(n_{\min},t) - n_mJ^{SS}_{ik}(n_m,t) + \rho_{ik}(Z_{ik}D_iC_i - Z_{vk}D_vC_v) - \rho_{dk}\int_{n_{\min}}^{n_m} nf_{ik}(n,t)W_k(n,n_m)dn. \quad (15)$$

Here ρ_{ik} is the line density of loops of kth class, and

$$J^{ss}_{ik}(n,t) = V_{ik}(n)f_{ik}(n,t) - \frac{\partial}{\partial n}[D_{ik}(n)f_{ik}(n,t)] \quad (16)$$

is the flux of the interstitial loops in size space. The physical meaning of each term in Eq. (15) is quite obvious from the foregoing.

Under the steady-state conditions there should be a balance between the loop creation and destruction, and, consequently, the total interstitial content of the loops should be conserved, i.e., $dQ_{ik}(t)/dt = 0$. This means that interstitials accumulating in the loops only contribute to the total strain rate in the transient regime. The steady strain rate is the result of the climb and recovery of network dislocations, which we will consider in the following subsection.

2.3. Straining due to loop growth, dislocation climb and recovery

From Eq. (15), interstitial loops joining the network dislocation population increase the total network line density at the rate $2\pi r_i(n_m)J^{ss}_{ik}(n_m,t)/\Omega$. In addition, the stress-induced anisotropy inherent in the Frank loop population also propagates into the network dislocation density when they unfault [5]. On the destructive side, climbing network dislocations may mutually cancel, for example, via the dipole mechanism [45,46]. Adopting the simple model for the dislocation recovery via dipole cancellation by climb, the conservation equation for the network line density ρ_{dk} of the kth class can be written as [26,42]

$$\frac{d\rho_{dk}}{dt} = 2\pi r_i(n_m)J^{ss}_{ik}(n_m,t)/\Omega - |V_{dk}|\rho^{3/2}_{dk}, \quad (17)$$

where

$$V_{dk}(n) = \frac{1}{b}\left(Z^{(N)}_{ik}D_iC_i - Z^{(N)}_{vk}D_vC_v\right) + \frac{1}{b}\int_{n_{\min}}^{n_m} nf_{ik}(n,t)W_k(n,n_m)dx \quad (18)$$

is the climb velocity of the network dislocations. $Z^{(N)}_{jk}$ is the reaction constant between network dislocations of the kth class and point defects.

The strain rate in the α direction due to the climb of network dislocations and the accumulation of interstitials in the loops can be calculated from the equation

$$\frac{d\varepsilon_\alpha}{dt} = \sum_k\left(\dot{Q}_{ik} + V_{dk}\rho_{dk}b\right)\cos^2\beta_{k\alpha}, \quad (19)$$

where $\beta_{k\alpha}$ is the angle made by the Burgers vector of dislocations of the kth class with the α direction.

The set of Eqs. (1) and (17) describes the evolution of the dislocation component of microstructure. For these equations to have a unique solution, equations to describe the concentrations of freely migrating point defects C_j are needed. The corresponding steady-state rate equations have the well-known form:

$$G - \sum\nolimits_k(\varepsilon_{ik}G - n_{\min}J^{ss}_{ik}(n_{\min})) - D_iC_i\left(k^2_{ci} + \sum\nolimits_k(Z_{ik}\rho_{ik} + Z^{(N)}_{ik}\rho_{dk})\right) = 0, \quad (20)$$

$$G - D_vC_v\left(k^2_{cv} + \sum\nolimits_k(Z_{vk}\rho_{ik} + Z^{(N)}_{vk}\rho_{dk})\right) = 0. \quad (21)$$

Here k^2_{cj} is the total sink strength of other sinks, such as the voids, present in the damage microstructure. In Eq. (20) we also assume that interstitial clusters shrinking below the minimum size $n_{\min}$ at the rate $J^{ss}_{ik}(n_{\min})$ spontaneously dissolve, and the corresponding number of free interstitials $n_{\min}J^{ss}_{ik}(n_{\min})$ is added to the population of mobile defects.

While swelling is very sensitive to material and environmental variables, such as temperature, stress, alloy type, cold work and composition, the experimental instantaneous creep rate appears to depend only on the applied stress and the instantaneous swelling rate [23,24]. This allows us to simplify the analysis in the present work by treating the void sink strength k^2_{jc} as a parameter describing the rate of vacancy accumulation in the alternate sinks. By varying this parameter, we are able to calculate steady-state creep rates for the corresponding void swelling rates.

In the following, without loss of generality, we restrict ourselves to only consider the stress effects of elastodiffusion [11], which causes a bias differential due to diffusion anisotropy difference (DAD) between the vacancies and interstitials according to

$$Z_{jk}(\sigma_{ml}) = Z^0_j\left(1 - \frac{(p^{(j)}_1 - 1)P^{(j)}}{16kT}\frac{\sigma}{\mu}\left[1 - \sum_m U_m\cos^2\lambda^{(m)}_k\right]\right), \quad (22)$$

where Z_j^0 is the reaction constant in the absence of stress, σ is the trace of the uniform external applied stress σ_{ml}, $P^{(j)}$ is one-third of the trace of elastic dipole tensor $P_{ml}^{(j)}$ of point-defect, $p_m^{(j)}$, $m = 1$ to 3, are normalized eigenvalues of $P_{ml}^{(j)}$ such that $\Sigma_m p_m^{(j)} = 3$, U_m is the mth normalized eigen value of the external stress tensor σ_{ml} such that $\Sigma_m U_m = 3$, μ is the shear modules, $\lambda_k^{(m)}$ is the angle that the Burgers vector of loops of the kth class makes with the mth eigen vector of σ_{ml}.

In a similar way, the reaction constant between point defects and network dislocations can be written as

$$Z_{jk}^{(N)}(\sigma_{ml}) = Z_j^0\left(1 + \frac{(p_1^{(j)} - 1)P^{(j)}}{8kT}\frac{\sigma}{\mu}\left[1 - \sum_m U_m \cos^2\lambda_k^{(m)}\right]\right). \quad (23)$$

In the case of network dislocations $\lambda_k^{(m)}$ is the angle between the mth eigen vector of σ_{ml} and the line direction of network dislocations of the kth class.

For the uniaxial stress $\sigma_{ml} = \sigma\delta_{1m}\delta_{ml}$, the reaction constants given by Eqs. (22) and (23) take the form

$$Z_{jk}(\sigma) = Z_j^0\left(1 - \frac{(p_1^{(j)} - 1)P^{(j)}}{16kT}\frac{\sigma}{\mu}\left[1 - 3\cos^2\lambda_{kl}\right]\right), \quad (24)$$

$$Z_{jk}^{(N)}(\sigma) = Z_j^0\left(1 + \frac{(p_1^{(j)} - 1)P^{(j)}}{8kT}\frac{\sigma}{\mu}\left[1 - 3\cos^2\lambda_{kN}\right]\right) \quad (25)$$

where λ_{kl} and λ_{kN} are, respectively, the angles made by the Burgers vector of loops and by the line direction of network dislocations of the kth class with the stress direction.

We represent the dislocation structure by three classes of dislocations, one ($k = 1$) with Burgers vector aligned with the external stress ($\lambda_{kl} = 0$, $\lambda_{kN} = \pi/2$) and two non-aligned (classes $k = 2$, 3; $\lambda_{kl} = \pi/2$, $\lambda_{kN} = 0$). According to Eqs. (24) and (25), the reaction constants for the three classes can be written respectively as

$$Z_{j1}(\sigma) = Z_{j1}^{(N)}(\sigma) = Z_j^0\left(1 + \frac{(p_1^{(j)} - 1)P^{(j)}}{8kT}\frac{\sigma}{\mu}\right), \quad (26)$$

$$Z_{j2}(\sigma) = Z_{j3}(\sigma) = Z_j^0\left(1 - \frac{(p_1^{(j)} - 1)P^{(j)}}{16kT}\frac{\sigma}{\mu}\right), \quad (27)$$

$$Z_{j2}^{(N)}(\sigma) = Z_{j3}^{(N)}(\sigma) = Z_j^0\left(1 - \frac{2(p_1^{(j)} - 1)P^{(j)}}{8kT}\frac{\sigma}{\mu}\right). \quad (28)$$

When $Z_{j2}(\sigma) = Z_{j3}(\sigma)$ and $Z_{j2}^{(N)}(\sigma) = Z_{j3}^{(N)}(\sigma)$, Eq. (1) becomes identical for the dislocation classes $k = 2$ and $k = 3$. So is Eq. (17). Thus, in the simplest case the total number of equations, which has to be solved, can be reduced from 8 to 6. They are the two Fokker–Planck equations (1) for the aligned and non-aligned loops, two equations (17) for the aligned and non-aligned network dislocations plus conservation Eqs. (20) and (21). It is also worth noting that values of the corresponding terms, which are calculated with Eqs. (1) and (17) for the non-aligned dislocations, should enter the conservation equations with a factor of 2.

3. Results

To facilitate comparison between model and experiment, stainless steel samples under a uniaxial tensile stress, i.e., $\sigma > 0$, are considered. Material parameters are listed in Table 1. The results are presented and discussed in the following subsections.

3.1. Dislocation structure and deformation in the absence of swelling

In Fig. 1, the time evolution of the dislocation densities of the aligned and non-aligned network is shown in the absence of swelling for various values of the applied stress. In general, the densities of both types of dislocations decrease with time and, consistent with the absence of swelling, the total volume remains unchanged, i.e.,

$$\dot{\varepsilon}_1 + \dot{\varepsilon}_2 + \dot{\varepsilon}_3 = \dot{\varepsilon}_1 + 2\dot{\varepsilon}_2 = 0. \quad (29)$$

Under the uniaxial stress, the original isotropic dislocation structure evolves anisotropically, yielding a dislocation structure that has a distinctly higher density for the aligned class compared with the non-aligned classes. The degree of the anisotropy increases with the applied stress. In Fig. 1, at a neutron dose of 30 NRT dpa, the proportion of aligned dislocations increases monotonically from 33% to 47%, 62% and 78% for increasing stresses of 50, 100 and 200 MPa, respectively.

Absent swelling, the positive climb of the aligned dislocations must be provided by the interstitials "borrowed" from the non-aligned dislocations that have lower biases, which effectively serve as net vacancy sinks. Under such circumstances, an increase in the network line density due to the unfaulting cannot occur with the non-aligned loops i.e., $J_{i2,3}^{ss}(n_m, t) \cong 0$. According to Eq. (17), the non-aligned network dislocation density decreases with time. Indeed, due to the larger amount of the interstitials that has to

Table 1
Material parameters for SS used in the calculations.

Parameter	Value
Burgers vector, b [47]	2.07×10^{-10} m
Atomic volume, Ω [47]	1.15×10^{-29} m^3
Trace of interstitial dipole tensor [48]	63.0 eV
Trace of vacancy dipole tensor [48]	−2.82 eV
Normalized eigenvalue of SIA dipole tensor, $p_1^{(i)}$ [48]	1.5
Normalized eigenvalue of vaccum dipole tensor, $p_1^{(v)}$ [48]	2.73
Shear modulus, μ	60 GPa
Intracascade interstitial clustering fraction, ε_{ik}	0.4/3
Initial content of PICs, n_{ig}	10
Minimum size of interstitial cluster, $n_{\min}$	4
Maximum loop radius, $r_i(n_m)$	40 nm
Average number of point defects per cascade, N_d	100
Intracascade recombination fraction	0.85

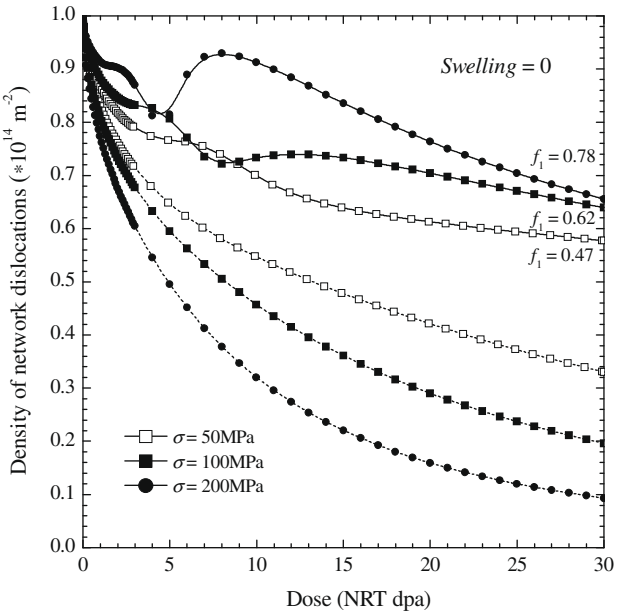

Fig. 1. Evolution of the aligned ρ_{d1} (solid lines) and non-aligned $\rho_{d2,3}$ (dashed lines) line densities of network dislocations for the various stress levels at the zero total swelling (total initial density of network dislocations $\rho_d(t = 0) = 3 \times 10^{14}$ m^{-2}). Values of $f_1 = \rho_{d1}/\rho_d$ indicate the fractions of aligned network dislocations at the dose 30 NRT dpa.

be "borrowed", this decrease accelerates with increasing stresses. The loss of non-align dislocations naturally also leads to the loss of aligned dislocations, when the source of interstitials they can "borrow" from dwindles.

To understand in greater detail the relatively complex behavior of the evolution of the aligned network dislocations, we plot in Fig. 2 the flux of align loops joining the network dislocations as a function of time (dose). The flux vanishes during the initial incubation period, at the end of which it quickly increases, peaks, and then decline with increasing dose to a steady-state value independent of the stress. During the incubation period, the aligned loops are generally not sufficiently large to be incorporated into the network. Consequently, both aligned and non-aligned network dislocation densities decrease with time, regardless of the sign of the dislocation climb velocity V_{dk}, being dominated by mutual cancellation (see Eq. (17)). Nevertheless, the decrease slows down when the climb velocity V_{dk} vanishes, producing the "knees" in the aligned dislocations during the incubation. At the end of the incubation period, the aligned loops start interacting with the network and unfault. The flux of the aligned dislocation loops joining the network rises sharply (see Fig. 2). The resulting peak in the loop flux is reflected in the peaked aligned network dislocation density in Fig. 1.

Both the growth of aligned loops and the climb of existing aligned network dislocations have to rely on "borrowed" interstitials. With the decreasing densities of non-aligned network dislocations, the amount of interstitials that can be "borrowed" from them also decreases with time. The number of aligned interstitial loops joining the network starts to drop shortly after the initial rise after the incubation (Fig. 2), leading to the reduction of line density of the aligned dislocations seen in Fig. 1.

Absent voids, non-aligned dislocations substitute as net vacancy sinks. Theoretically, a continuous decline of the dislocation line density will lead to their eventual decimation, at which point irradiation creep stops. However, in practice this scenario is rarely realizable because after an initial irradiation dose of ~20–30 NRT dpa, significant void swelling usually starts developing [49–52]. The decline of non-aligned dislocation density also means that in the empirical creep law proposed by Garner et al. [49,51,52]

$$\frac{(\dot{\varepsilon}_1 - \dot{S}/3)}{\sigma} = B_0 + D\dot{S}, \tag{30}$$

the creep compliance B_0 is actually dose dependent in the absence of swelling. In Eq. (30), D is the creep–swelling coupling coefficient, and $\dot{S}$ is the instantaneous swelling rate. Furthermore, since the dislocation densities $\rho_{d2,3}$ drop faster with increasing stress (Fig. 1), the creep strain at higher stress levels would start to saturate earlier. Thus, the value of B_0 extracted from the experimental measurements at similar doses should decrease with increasing applied stress. This conclusion is in agreement with the existing experimental observations [53,54].

In Fig. 3, the calculated creep strain in the stress direction $\varepsilon_1(t)$ is plotted as a function of irradiation dose for various applied stresses. The time averaged values of the creep compliance B_0 for σ = 200 MPa changes from 1.1×10^{-6} at 20 NRT dpa to 0.86×10^{-6} MPa^{-1}/NRT dpa at 30 NRT dpa. For σ = 50 MPa these values changes to 1.46×10^{-6} and 1.40×10^{-6} MPa^{-1}/NRT dpa, respectively. These calculated values are in very good agreement with the typical range of experimental creep compliance of $B_0 \sim 10^{-6}$ MPa^{-1}/NRT dpa in the absence of swelling [21–24,53–55].

3.2. Dislocation structure development in the presence of swelling

In the presence of swelling, the nucleation and growth of voids provides an ample source of interstitials for the climbing dislocations, mitigating their need to "borrow" from one another. At a sufficiently high swelling rate, this source becomes strong enough to supply all interstitials needed for the climb of the aligned dislocations. In Fig. 4, the fluxes of loops joining the network dislocations are shown as a function of swelling rate for various applied stresses. It can be seen that above a swelling rate of $\dot{S} \sim 0.1$–0.2%/NRT dpa, the non-aligned loops may already be able to grow to sizes large enough to interact with the network, unfault, and add to the line densities of the non-aligned network $\rho_{d2,3}(t)$ as shown in Fig. 5.

We emphasize that the total line densities of network dislocations in Fig. 5 are calculated. That they are well within the typical

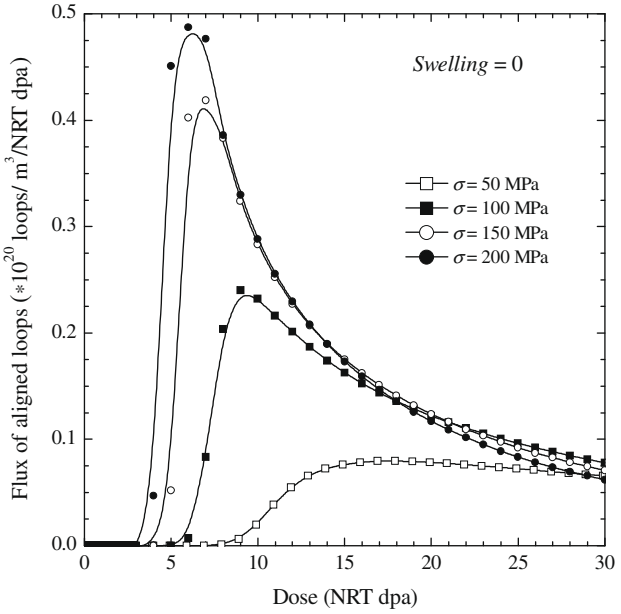

Fig. 2. Flux $J_{i1}^{ss}(n_m, t)/\Omega$ of the aligned loops joining the network dislocations.

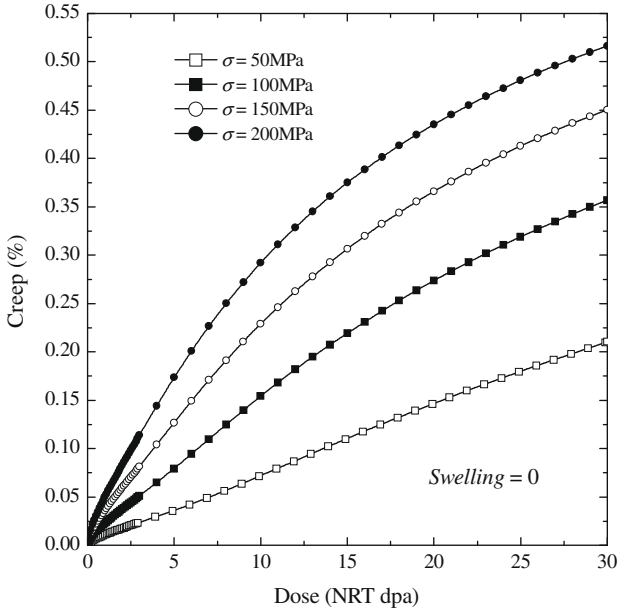

Fig. 3. Creep ε_1 in the stress direction as a function of irradiation dose for the various stress levels at the zero total swelling (total initial density of network dislocations $\rho_d(t=0) = 3 \times 10^{14}$ m^{-2}).

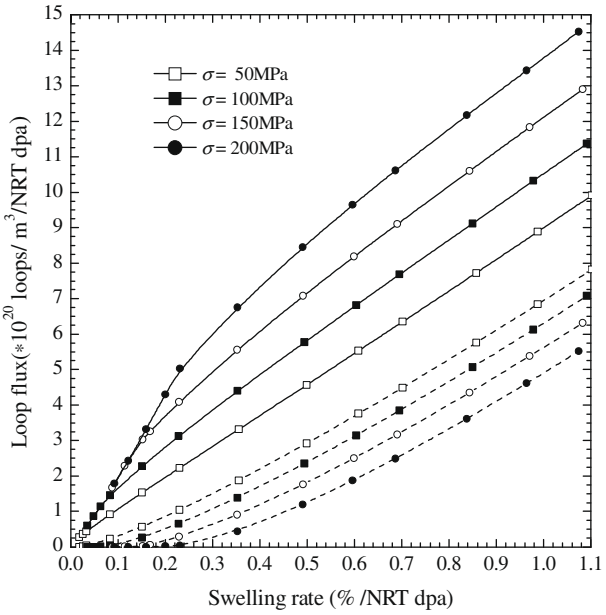

Fig. 4. Steady-state flux of the aligned loops $J^{ss}_{i1}(n_m,t)/\Omega$ (solid lines) and the non-aligned loops $J^{ss}_{i2}(n_m,t)/\Omega$ (dashed lines) joining the network dislocations as a function of the swelling rate for the various stress levels.

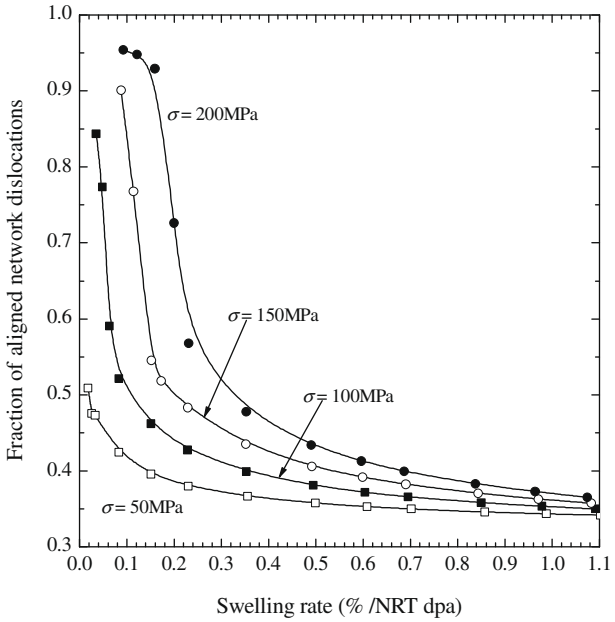

Fig. 6. Fraction $f_1(t) = \rho_{d1}(t)/\rho_d(t)$ of the aligned network dislocations as a function of the swelling rate for the various stress levels.

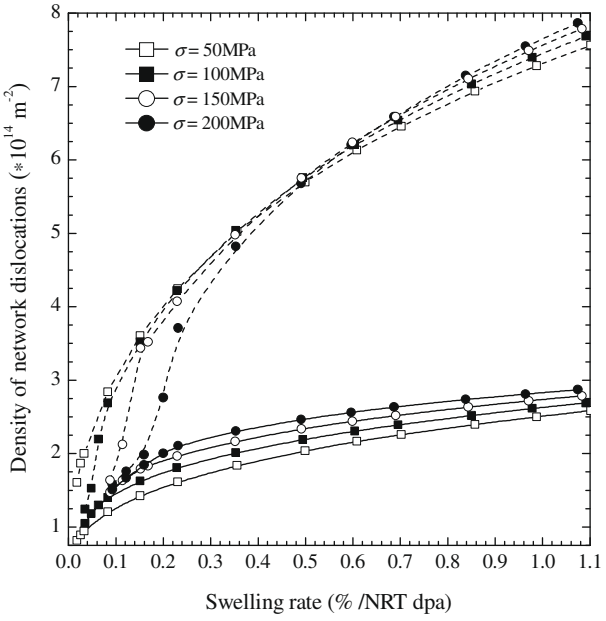

Fig. 5. Steady-state density of the aligned network dislocations ρ_{d1} (solid lines) and the total steady-state density of network dislocations $\rho_d(t) = \sum_{k=1}^{k=3}\rho_{dk}(t)$ (dashed lines) as functions of the swelling rate for the various stress levels.

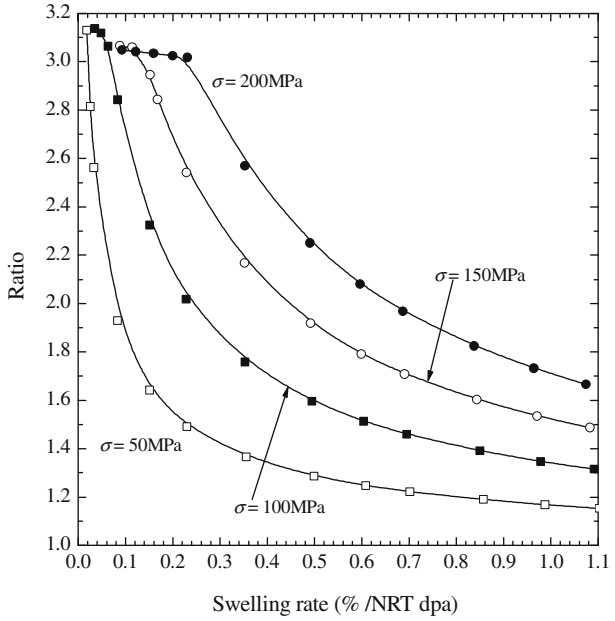

Fig. 7. Ratio of the total strain rate $\dot{\varepsilon}_1$ to the one-third of the swelling rate as a function of the swelling rate.

range of the experimental values observed in stainless steel [52] lends credibility to the loop nucleation and growth treatment presently undertaken.

In Fig. 6, the fraction of aligned network dislocations $f_1(t) = \rho_{d1}(t)/\rho_d(t)$ is plotted against the swelling rate, showing a monotonic decreasing function. As a result, the deformation rate due to SIG also decreases with increasing swelling rate. Indeed, for low swelling rates ($\dot{S} \sim 0.1\%$/NRT dpa), the dislocation structure shows maximum anisotropy ($f_1 \sim 1$ in Fig. 6) and the total deformation strain due to the sum of creep and swelling is realized mostly through the climb of the aligned dislocations.

In Fig. 7, the ratio of steady-state strain rate in the stress direction to that due to swelling (i.e., $\dot{\varepsilon}_1/(\dot{S}/3)$) is shown. Independent of the applied stress, the ratio attains a maximum value of ~3 in the low swelling rate regime, in good agreement with the experimental total diametral strain rates of stressed tubes at 400 °C, which swells at a steady rate of ~0.1%/NRT dpa [21–23,51,55].

In Fig. 8, it can be seen from the slopes of the curves that the creep rate increases linearly with the swelling rate at the onset of swelling (i.e., when the swelling rate is low). As the swelling rate increases, the creep rate tends to become saturated and makes a proportionately smaller contribution to the total strain rate. This explains why creep rates increase linearly with stress only up to

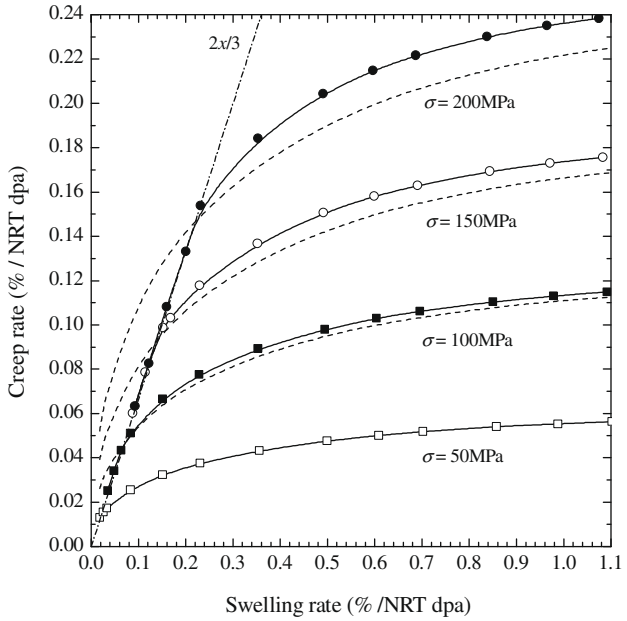

Fig. 8. Steady-state creep rate ($\dot{\varepsilon}_1 - \dot{S}/3$) versus swelling rate for the various stress levels. The dashed lines correspond to the creep rate for $\sigma = 50$ MPa multiplied by the factor of 2, 3 and 4, respectively.

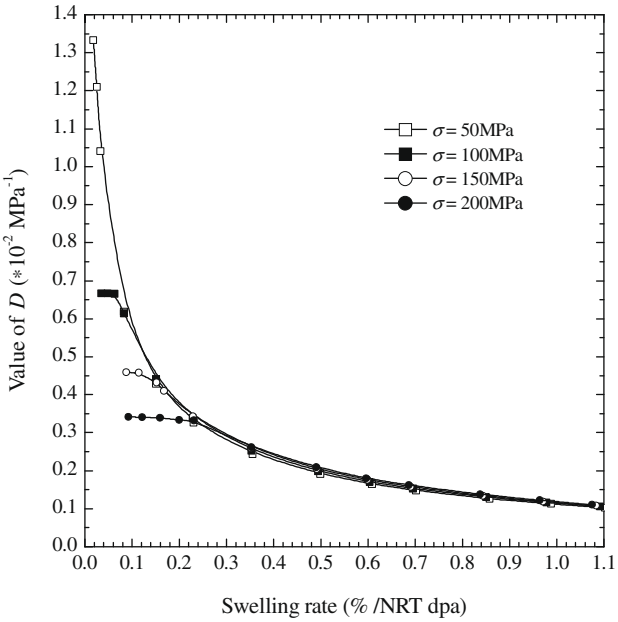

Fig. 9. The calculated value of D-coefficient in empirical relation (30) as a function of the swelling rate.

a certain maximum stress, beyond which further increase does not cause a proportionate increase in the strain rate [23]. These results are also consistent with the observation of Garner and co-workers [21,22,53] that creep rates first accelerate with the onset of swelling and then decline as the swelling rate increases. In this regard, we note that the absolute value of the creep rate ($\dot{\varepsilon}_1 - \dot{S}/3$) only tends to a saturated value, and does not actually decrease at high swelling rates. Thus, due to the reduction of the SIG effect as the swelling rate increases, there is a general tendency for the applied stress to become less effective in driving the creep deformation in the stress direction. This explains why creep equations derived from data in the low swelling rate regime would over-predict the creep rate in the high swelling rate regime, as noted in [55].

Using steady-state creep rates from Fig. 8, we can evaluate the swelling–creep coupling coefficient D that satisfies the empirical relationship (30). Since B_0 actually decreases with increasing dose, it should be set to zero in Eq. (30) for steady-state calculations. The results are shown in Fig. 9. It can be seen that D in Eq. (30) is not a constant, but decreases with increasing swelling rate. This is in good agreement with experiments [52,53], where D decreases from $D \approx 6 \times 10^{-3}$ MPa^{-1} at $\dot{S} \approx 0.1\%$/NRT dpa to $D \approx 2 \times 10^{-3}$ MPa^{-1} at $\dot{S} \approx 0.3\%$/NRT dpa.

The stress-dependent term in brackets in the reaction constants in Eqs. (26)–(28) is much smaller than unity for the stresses considered. In a first approximation both the climb-rate differentials and the creep rates should be linear functions of the applied stress. The numerical results in Figs. 8 and 9 show that this is indeed the case for a wide range of swelling rates. A deviation from the linear dependence of creep on the stress takes place when the swelling rates are low, i.e., when the dislocation structure is very anisotropic ($f_1 >> f_{2,3}$), and most of the strain is provided by the climb of the aligned dislocations only. As a result, $\dot{\varepsilon}_1 - \dot{S}/3 \approx 2\dot{S}/3$ (Fig. 8), and there is no explicit dependence on the stress. The dependence is only implicit, through the maximum value of the swelling rate, at which the dislocation structure still shows the maximum anisotropy. It is clear from Fig. 9 that this maximum value decreases with stress.

4. Discussions

Decades of studies of in-reactor creep deformation in stainless steels consistently showed that irradiation creep is strongly coupled to the void swelling of the material. Foster et al. [15] were among the first to propose an empirical equation in which the creep rate is the sum of two components: one that is swelling-independent, and the other that is directly proportional to the swelling rate. Many subsequent experiments [15–25] yield results that support this observation. The I-creep model has been used to account for the coupling [18,19] because it predicts a creep rate proportional to stress and swelling rate. However, observable correlations between irradiation creep and the concomitant microstructural development seem to point to complexities beyond the grasp of this model. Indeed, Garner and co-workers [21,22,53] observed that creep rates first accelerate with the onset of swelling and then decline as the swelling rate increases. Creep equations developed from data on highly pressurized tubes over-predict the creep observed in fuel pins where the onset of void swelling precedes the development of significant stress levels [55]. Creep rates increase linearly with stress only up to a maximum stress, beyond which any further increase of the applied stress does not cause a proportionate increase in the strain rate [23]. The most revealing observation is the anisotropy of the dislocation structure that accompanies irradiation creep [20–25], and the continuation of creep over a substantial period of time, even after the applied stress is removed [5].

In Section 3, it can be seen that the straining process involving both swelling and creep is derived from the climb of the same dislocation structure, evolving under the combined action of the applied stress and the neutron irradiation. The swelling strain comes from the volumetric component, and the creep from the deviatoric component, and that is all. The onset of void swelling segregates out the vacancies, which would otherwise annihilate SIAs in the loops or at the dislocations network, slow down dislocation climb and reduce the deformation rate. For typical void swelling rates in stainless steels, this source of freed-up SIAs produces a very strong effect. Comparing Figs. 2 and 4, it is clear that the presence of swelling leads to a much higher generation rate of new network dislocations. Thus, even without an applied stress, a swelling

rate as low as 0.05%/NRT dpa might produce an axial strain of 0.5% at 30 NRT dpa, which could be as large as that created by an applied stress of 200 MPa in the absence of swelling (see Fig. 3). To further illustrate the effect of swelling on creep, Fig. 8 shows that even for a relatively low swelling rate of ~0.1%/NRT dpa the strain rate in the stress direction could be increased by several times.

In Section 3.2, we can also see that swelling makes a significant and direct contribution to the deviatoric strain as long as the dislocation structure is anisotropic. Thus, even if the applied stress is removed and all dislocations climb at exactly the same speed, the deviatoric component of the strain rate will remain in the presence of swelling until the dislocation anisotropy is totally wiped out. The specimen deformation in this case is entirely due to SIPA-induced growth (SIG) [12–14]. These results explain very well the correlation between dislocation anisotropy and irradiation creep [4,5,21–25], and the apparent memory of stress that continue to produce creep even after the applied stress is removed [5].

While the presence of voids enhances creep by facilitating the operation of SIG, it also trims down the amount of interstitial "borrowing" from the non-aligned dislocations and tends to impede the development of dislocation anisotropy under the applied stress. This is seen in Figs. 5 and 6, where the fraction of the aligned dislocations at steady-state sharply drops when the swelling rate increases from 0.1% to 0.2 %/NRT dpa. Indeed, at $\dot{S} \cong 1\%$/NRT dpa the dislocation structure becomes practically isotropic, and there is hardly any direct creep contribution from swelling, i.e., SIPA-induced growth vanishes.

From the foregoing it follows that at low swelling rates (such as at temperatures below the high swelling regime, or at the onset of swelling) void swelling accelerates the "creep" rate via SIG, mainly due to the developing dislocation anisotropy. However, at high swelling rates, the dislocation anisotropy decreases and the SIG rate stops to increase. This is reflected in the creep–swelling coupling coefficient D which varies inversely with the swelling rate, decreasing from a value of $D > 10^{-2}$ MPa^{-1} at a swelling rate of 0.05%/NRT dpa to a value of $D \sim 10^{-3}$ MPa^{-1} at a swelling rate of ~1%/NRT dpa (Fig. 9). This behavior of D is in good quantitative agreement with experiments [51–53]. It also means that the limiting value of $D \approx 0.6 \times 10^{-2}$ MPa^{-1} derived from the experiments is representative of all low swelling rate cases with $\dot{S} \sim 0.1\%$/NRT dpa [21–24,52–53]. The reduction of the anisotropy of dislocation structure at high fluence, where swelling rate is high, has been reported as well [3,5].

Although the creep–swelling coupling coefficient D decreases with increasing swelling rate, the corresponding creep compliance given by the product $D\dot{S}$ does not. In other words, despite the reduced responsiveness of the deviatoric strain rate to the swelling rate, the magnitude of the creep rate does not decrease at high swelling rates (Fig. 8). This is because the net interstitial flux to the dislocations increases with the swelling rate and compensates for the lost anisotropy. Nevertheless, the gradual loss of relative importance of a constant creep rate in an increasing total (i.e., swelling and creep) strain rate is hardly surprising (see Figs. 7 and 8). Experimentally, the reduced sensitivity of the total strain rate on the stress at high swelling rate is a well-established observation and has been interpreted as creep cessation at high swelling [5,51].

We also note that qualitatively, and to a certain extent quantitatively, the numerical results obtained in the present paper agree reasonably well with analytical considerations in [13] and [56]. Making the assumption that the stress only affects the steady-state loop-number density but not the loop size and using the stress-induced diffusion anisotropies of vacancies and self-interstitials, the authors of [13] and [56] calculate the relative dislocation densities f_k as a function of the stress and swelling rate. From this they can determine the deviatoric strain rate due to SIG, without having to calculate the network line densities ρ_{dk} and the fluxes of the interstitial loops joining the network. Despite the large simplification, the constraints imposed by the law of matter conservation make sure that the general behavior of the creep–swelling coupling coefficients agree with that shown in Fig. 9.

Unlike the present results, the values of B_0 in the absence of swelling calculated in [13] and [56] are independent of dose, which can be traced to the implicit assumption that non-aligned dislocations always exist. As a result, the steady-state solutions obtained becomes unphysical when the swelling rate is too low. However, within the framework of [13] and [56] it can be easily shown that, without the artificial limitation, a continuous steady-state solution for any finite value of the swelling rate exists with a zero steady-state value of B_0. In other words, in agreement with the present results and the law of matter conservation, at $t \to \infty$ the time average value of the creep compliance B_0 tends to zero.

5. Summary and conclusions

In this paper, we physically model dislocation structure development in stainless steel under the combined actions of fast-neutrons and an external applied stress from the anisotropic nucleation and growth of multi-classes of cascade generated dislocation loops. We use the Fokker–Planck equation approach to include the stochastic effects due to diffusion jumps and cascade initiation, which is particularly important for the nucleation and growth of interstitial loops under the operation of production bias. In our model, bias differential among dislocations of different classes is created by the stress-induced diffusion anisotropy. With atomistically calculated point-defect properties, the total deformation strain rates due to dislocation climb under different uniaxial stresses is calculated for stainless steel for various void swelling rates. Our results show that:

(1) Under the combined actions of fast-neutrons and an external applied stress, an initially isotropic dislocation structure is changed into an anisotropic one. The fraction of the aligned network dislocations decreases strongly from close to 100% in the absence of swelling to approaching 33% for a swelling rate beyond ~0.5%/NRT dpa. The decrease is faster for lower stresses.
(2) The total deformation due to the dislocation climb can be separated into volumetric and deviatoric components, responsible respectively for swelling and creep. The steady-state creep can be very well represented by the equation $\dot{\varepsilon}_1 = (B_0 + D\dot{S})\sigma$, with a creep compliance that is a linear function of the swelling rate, which is responsible for the coupling between creep and swelling. The swelling-independent contribution can be traced to the climb-rate difference between the aligned and the non-aligned dislocations i.e., SIPA, while the swelling-dependent contribution comes from the stress-induced anisotropy of the dislocation structure, i.e., SIG. Except for very small swelling rates, the SIG compliance is several times larger than the SIPA contribution and is relatively constant, i.e., independent of the applied stress and the swelling rate.

The creep behaviors predicted based on this model are in good agreement with a variety of experiments, both qualitatively and quantitatively, and describes very well the coupled behavior of irradiation creep and void swelling in stainless steels via the anisotropic development of the dislocation structure under stress.

Acknowledgement

The authors are grateful for funding support by research grant PolyU5305/07E.

References

[1] H.R. Brager, F.A. Garner, G.L. Guthrie, J. Nucl. Mater. 66 (1977) 301.
[2] F.A. Garner, W.G. Wolfer, H.R. Brager, in: J.A. Sprague, D. Kramer (Eds.), Effects of Radiation on Structural Materials, ASTM STP 683, ASTM, 1979, p. 160.
[3] D.S. Gelles, F.A. Garner, H.R. Brager, in: D. Kramer, H.R. Brager, J.S. Perrin (Eds.), Effects of Radiation on Materials, ASTM STP 725, ASTM, 1981, p. 735.
[4] D.S. Gelles, in: F.A. Garner, J.S. Perrin (Eds.), Effects of Radiation on Materials, ASTM STP 870, ASTM, Philadelphia, 1985, p. 98.
[5] F.A. Garner, G.S. Gelles, J. Nucl. Mater. 159 (1988) 286.
[6] C.H. Woo, in: S. Yip (Ed.), Handbook of Materials Modelling, Springer, Netherlands, 2005, p. 959.
[7] P.T. Heald, M.V. Speight, Philos. Mag. 29 (1974) 1075.
[8] R. Bullough, J.R. Willis, Philos. Mag. 31 (1975) 855.
[9] W.G. Wolfer, M. Ashkin, J. Appl. Phys. 47 (1976) 791.
[10] C.H. Woo, J. Nucl. Mater. 80 (1979) 132.
[11] C.H. Woo, J. Nucl. Mater. 120 (1984) 55.
[12] C.H. Woo, Philos. Mag. A 42 (1980) 551.
[13] C.H. Woo, F.A. Garner, R.A. Holt, in: A.S. Kumar, D.S. Gelles, R.K. Nanstad, E.A. Little (Eds.), Effects of Radiation on Materials, ASTM STP 1175, ASTM, Philadelphia, 1993, p. 27.
[14] C.H. Woo, J. Nucl. Mater. 225 (1995) 8.
[15] J.P. Foster, W.G. Wolfer, A. Biancheria, A. Boltax, in: Proceedings, BNES Conference on Irradiation Embrittlement and Creep in Fuel Cladding and Core Components, London, UK, 1973, p. 273.
[16] G.L. Wire, J.L. Straalsung, J. Nucl. Mater. 64 (1977) 254.
[17] B.A. Chin, J.L. Straalsung, G.L. Wire, J. Nucl. Mater. 80 (1979) 144.
[18] W. Schneider, K. Herschback, K. Ehrlich, in: H.R. Brager, J.S. Perrin (Eds.), Effects of Radiation on Materials, ASTM STP 782, ASTM, 1982, p. 30.
[19] J.L. Boutard, Y. Carteret, R. Cauvin, Y. Guerin, A. Maillard, in: Proceedings, BNES Conference on Dimensional Stability and Mechanical Behaviour of Irradiated Metals and Alloys, 1983, p. 109.
[20] D.S. Gelles, R.J. Puigh, in: F.A. Garner, J.S. Perrin (Eds.), Effects of Radiation on Materials, ASTM STP 870, ASTM, Philadelphia, 1985, p. 19.
[21] F.A. Garner, D.L. Porter, J. Nucl. Mater. 155–157 (1988) 1006.
[22] M.B. Toloczko, F.A. Garner, C.R. Eiholzer, J. Nucl. Mater. 191–194 (1992) 803.
[23] D.L. Porter, G.D. Hudman, F.A. Garner, J. Nucl. Mater. 179–181 (1991) 581.
[24] F.A. Garner, J.R. Puigh, J. Nucl. Mater. 179–181 (1991) 577.
[25] D.L. Porter, E.L. Wood, F.A. Garner, in: N.H. Packen, R.E. Stoller, A.S. Kumar (Eds.), Effects of Radiation on Materials, ASTM STP 1046, vol. 2, ASTM, Philadelphia, 1990, p. 551.
[26] A.A. Semenov, C.H. Woo, Philos. Mag. 83 (2003) 3765.
[27] A.A. Semenov, C.H. Woo, J. Nucl. Mater. 323 (2003) 192.
[28] C.H. Woo, B.N. Singh, Phys. Stat. Sol. (b) 159 (1990) 609; C.H. Woo, B.N. Singh, Philos. Mag. A 65 (1992) 889.
[29] B.N. Singh, A.J.E. Foreman, Philos. Mag. A 66 (1992) 975.
[30] B.N. Singh, S.I. Golubov, H. Trinkaus, A. Serra, Yu.N. Osetsky, A.V. Barashev, J. Nucl. Mater. 251 (1997) 107.
[31] B.N. Singh, S.I. Golubov, H. Trinkaus, J. Nucl. Mater. 276 (2000) 78.
[32] Yu.N. Osetsky, D.J. Bacon, A. Serra, B.N. Singh, S.I. Golubov, J. Nucl. Mater. 276 (2000) 65.
[33] W. Frank, A. Seeger, Mater. Sci. Forum 15–18 (1987) 57.
[34] T.S. Hudson, S.L. Dudarev, A.P. Sutton, Proc. R. Soc. London A 460 (2004) 2457.
[35] T.S. Hudson, S.L. Dudarev, A.P. Sutton, J. Nucl. Mater. 329–333 (2004) 971.
[36] A.A. Semenov, C.H. Woo, Phys. Rev. B 74 (2006) 024108; A.A. Semenov, C.H. Woo, Appl. Phys. A 84 (2006) 261.
[37] A.A. Semenov, C.H. Woo, W. Frank, Appl. Phys. A 93 (2008) 365.
[38] S.L. Dudarev, A.A. Semenov, C.H. Woo, Phys. Rev. B 67 (2003) 094103.
[39] A.A. Semenov, C.H. Woo, Appl. Phys. A 74 (2002) 639.
[40] S.L. Dudarev, A.A. Semenov, C.H. Woo, Phys. Rev. B 70 (2004) 094115; S.L. Dudarev, A.A. Semenov, C.H. Woo, Fusion Eng. Des. 75–79 (2005) 1031.
[41] C.A. English, M.L. Jenkins, MMM2008, in: Fourth International Conference of Multiscale Materials Modeling, October 27–31, 2008, Tallahassee, Florida, USA.
[42] A.A. Semenov, C.H. Woo, Appl. Phys. A 67 (1998) 193.
[43] A.A. Semenov, C.H. Woo, Appl. Phys. A 69 (1999) 445.
[44] A.A. Semenov, C.H. Woo, J. Nucl. Mater. 233–237 (1996) 1045.
[45] B.B. Glasgow, W.G. Wolfer, in: F.A. Garner, J.S. Perrin (Eds.), Effects of Radiation on Materials, ASTM STP 870, ASTM, Philadelphia, 1985, p. 453.
[46] J.R. Matthews, M.W. Finnis, J. Nucl. Mater. 159 (1988) 257.
[47] R.E. Stoller, G.E. Odette, in: F.A. Garner, N.H. Packan, A.S. Kumar (Eds.), Effects of Radiation on Materials, ASTM STP 955, ASTM, Philadelphia, 1987, p. 371.
[48] H.R. Schober, J. Phys. F7 (1977) 1127.
[49] F.A. Garner, J. Nucl. Mater. 122–123 (1984) 459.
[50] D.L. Porter, F.A. Garner, in: F.A. Garner, J.S. Perrin (Eds.), Effects of Radiation on Materials, ASTM STP 870, ASTM, Philadelphia, 1985, p. 212.
[51] M.B. Toloczko, F.A. Garner, J. Nucl. Mater. 212–215 (1994) 509.
[52] F.A. Garner, Materials Science and Technology: A Comprehensive Treatment, vol. 10A, VCH Publishers, 1994. Chapter 6.
[53] M.B. Toloczko, F.A. Garner, C.R. Eiholzer, J. Nucl. Mater. 212–215 (1994) 604.
[54] E.R. Gilbert, F.A. Garner, J. Nucl. Mater. 367–370 (2007) 954.
[55] F.A. Garner, D.L. Porter, B.J. Makenas, J. Nucl. Mater. 148 (1987) 279.
[56] C.H. Woo, F.A. Garner, J. Nucl. Mater. 191–194 (1992) 1309.